A 3D-Printed Multi-Material GRIN Lens with an Integrated Matching Layer at 20 GHz

Simon P. Hehenberger[$#1], Stefano Caizzone[$2], Alexander Yarovoy[#3]

[$]Institute for Communication and Navigation, German Aerospace Center (DLR), Germany

[#]Microwave Sensing, Signals and Systems, Delft University of Technology, Netherlands

{[1]simon.hehenberger, [2]stefano.caizzone}@dlr.de, [3]a.yarovoy@tudelft.nl

***Abstract* — The design, fabrication, and experimental validation of a gradient-index (GRIN) lens operating at 20 GHz is presented. Different realizations with and without matching layers at the input and output interfaces are compared. The lens design employs a semi-analytical approach to compute the desired permittivity distribution, which is realized using a periodic dielectric structure with a spatially modulated volumetric infill. The lens is manufactured via a multi-tool 3D printer utilizing two different dielectric materials for the core and matching layers, respectively. The lens design with and without the matching layer is experimentally verified. The comparison highlights the critical role of impedance matching at the interfaces, with the lens exhibiting superior performance when matching layers are incorporated. This work demonstrates the potential of multi-dielectric 3D printing for producing mmWave components, suggesting its applicability in future high-performance antenna systems.**

***Keywords* — Additive Manufacutring, Dielectric, Heterogeneous, GRIN Lens, Matching, Dielectric Crystal**

I. Introduction

As wireless communication technologies advance towards higher frequencies, particularly in the millimeter-wave range, the demand for efficient, compact, high-performance antenna components has grown significantly. Enabled through additive manufacturing (AM), gradient-index (GRIN) lenses, which employ spatially varying refractive indices to focus electromagnetic waves, have emerged as a key technology for a variety of applications in this frequency domain. GRIN lenses offer several advantages, including low profile, wide bandwidth, and superior focusing capabilities. In particular, flat GRIN lenses are attractive for mmWave systems due to their compact form factor and potential to minimize aberrations [1].

The design of GRIN lenses typically involves engineering the permittivity distribution within the lens material, which controls the wavefront of the transmitted signal. However, a significant challenge in GRIN lens design is impedance mismatch at the input and output interfaces, leading to reflections that degrade overall performance. One approach to mitigate this issue is using matching layers at the lens interfaces.

This work presents the design and fabrication of a flat GRIN lens operating at 20 GHz, comparing realizations with and without matching layers. The permittivity profile of the lens is calculated using a semi-analytical method and realized via periodic dielectric lattice based on superimposed spatial harmonics. The fabrication uses a multi-tool 3D printer capable of manufacturing up to four dielectric materials. The core of the lens is fabricated from ABS650, with a relative permittivity of $\varepsilon_{\text{r,ABS650}} = 6.5$, while the matching layers are realized using ABS300 with a relative permittivity of $\varepsilon_{\text{r,ABS300}} = 3$. The manufactured lenses with and without the integrated matching layer are experimentally verified regarding their far-field radiation patterns, specifically their realized gain values. The measurement results confirm the lenses' desired collimation effect and an increase in realized gain due to the integrated matching layer.

The remainder of this work is structured as follows: Section II presents the design approach to calculating the effective permittivity of the GRIN lens and elaborates on the design of the periodic lattice with spatially modulated volumetric infill. Section III explains the manufacturing process and the measurement setup for experimental characterization. Section IV provides a conclusion.

II. Design

A. Collimating GRIN Lens Design

We consider the simple case of a rotationally symmetric GRIN lens with diameter D at a distance F from its focal point O as depicted in Figure 1, with refractive index distribution $n(x) \in [n_{\min}\ n_{\max}]$, surrounded by empty space $n_{\text{in}} = n_{\text{out}} = 1$. An arbitrary ray with incident angle θ_{in} transmits through the lens from P_1 to P_2 and exits the lens with transmitted angle θ_{out}. The distance between the point P_2 and the desired equi-phase line is denoted as $L(x)$. The phase variation from the feed to the equi-phase wavefront for each ray should be equal to the ray passing through the lens center, expressed via

$$n_{\text{in}}F + n_{\max} + n_{\text{out}}L(0) = n_{\text{in}}\frac{F}{\cos\theta_{\text{in}}} + \int_{P_1}^{P_2} n\,ds + n_{\text{out}}L(x). \tag{1}$$

To simplify the design, the path integral inside the lens is approximated via a linear variation with a slope $k > 0$ of the permittivity profile $\varepsilon_{\text{r}}(x) = n(x)^2$ between the points P_1 and P_2. This allows to write

$$\varepsilon_{\text{r}}(x) - \varepsilon_r(x_2) = a(x_2 - x) \tag{2}$$

with

$$a = \frac{\varepsilon_{\text{r}}(x_1) - \varepsilon_{\text{r}}(x_2)}{x_2 - x_1}. \tag{3}$$

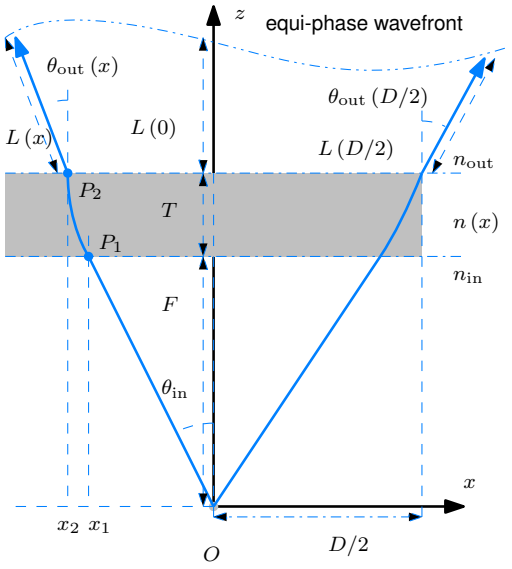

Fig. 1. Geometry of the flat GRIN lens.

This in turn provides a closed from solution for the path integral given by

$$\int_{P_1}^{P_2} nds = T\frac{\left(S_{\text{in}}^3/3 + 2S_{\text{out}}^3/3\right) + \left(\varepsilon_r(x_2) - S_{\text{out}}^2\right) S_{\text{in}}}{\sqrt{\varepsilon_r(x_2) S_{\text{out}}^2}\left(S_{\text{in}} - S_{\text{out}}\right)} - T\frac{\varepsilon_r(x_2) S_{\text{out}}}{\sqrt{\varepsilon_r(x_2) S_{\text{out}}^2}\left(S_{\text{in}} - S_{\text{out}}\right)} \tag{4}$$

with $S_{\text{in}} = n_{\text{in}}\sin\theta_{\text{in}}$ and $S_{\text{out}} = n_{\text{out}}\sin\theta_{\text{out}}$. For the simple case of a collimating lens the term $L(x)$ vanishes and all transmitted angles $\theta_{\text{out}} = 0$, allowing to rewrite equation (1):

$$n_{\text{in}}F + n_{\text{max}} = n_{\text{in}}\frac{F}{\cos\theta_{\text{in}}} + \int_{P_1}^{P_2} nds \tag{5}$$

which, with the application of equation (4), is a function of θ_{in} and $\varepsilon_r(x_2)$. With a given values for n_{max} and n_{min} [1] the thickness of the lens T can be found via

$$T = \frac{n_{\text{in}}F\left(\frac{1}{\cos\theta_{\text{in,max}}-1}\right)}{n_{\text{max}} - \frac{3\varepsilon_{\text{r,min}} - 2S_{\text{in,max}2}}{3\sqrt{\varepsilon_{\text{r,min}} - S_{\text{in,max}}}}} \tag{6}$$

with $\theta_{\text{in,max}} = \tan^{-1}\left[D/(2F)\right]$. Once T is found the values $\varepsilon_{\text{r}}(x)$ can be determined with equation (5).

B. Impedance Matching

For impedance matching we use a quarter wave transformer to match the wave impedance at the interfaces of the GRIN lens to the wave impedance of free space. Thus the permittivity of the matching slab is simply found via

$$\varepsilon_{\text{ML}} = \sqrt{\varepsilon_{\text{r}}(x)} \tag{7}$$

and the thickness of the matching layer h_{ML} is a quarter wavelength inside the material at center frequency.

[1] due to the permittivity of the print material and the minimum achievable volumetric infill

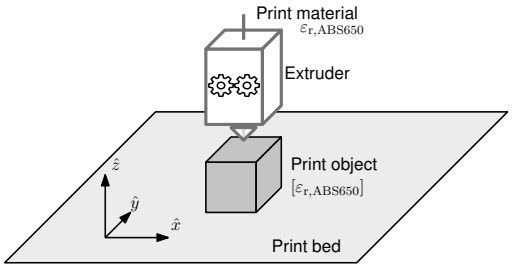

Fig. 2. Schematic representation of the additive manufacturing process using extrusion-based technology. Thermoplastic print material, in this case, ABS650 with isotropic relative permittivity $\varepsilon_{\text{r,ABS650}}$, is molten and extruded onto a heated print bed with the extruder moving along the $\hat{x}$ and $\hat{y}$ axis. Individual layers are stacked along the $\hat{z}$ axis. Imperfections during the print process result in an effective dielectric anisotropy introduced in the print part indicated via $[\varepsilon_{\text{r,ABS650}}]$.

C. Design Constraints and Material Realization

The extrusion-based additive manufacturing process creates a part through the extrusion of molten thermoplastic material onto a print bed, as schematically depicted in Figure 2, with the extruder moving along the $\hat{x}$ and $\hat{y}$ axis and stacking individual layers along the $\hat{z}$ axis. The extrusion of parallel lines and stacking of layers results in an inherent dielectric anisotropy in the printed part, which depends on the print material and the print settings during manufacturing [2]. In this work we utilize the thermoplastic materials ABS650 and ABS300 from Avient, which exhibit nominal permittivities of $\varepsilon_{\text{r, ABS650}} = 6.5$, $\varepsilon_{\text{r, ABS300}} = 3$ and a low loss tangent of $\tan\delta_{\text{ABS650}} = 0.0034$ $\tan\delta_{\text{ABS300}} = 0.0046$[2] for the core and matching layers of the lens. The effective permittivity tensor of a solid part printed from the ABS650/ABS300 material with an extrusion width of 0.2mm and a layer height of 0.12mm (as later utilized during the manufacturing) is characterized a waveguide measurement setup as described in [2] and measured to be

$$[\varepsilon_{\text{r,ABS650}}] = \begin{bmatrix} \varepsilon_{\hat{x}\hat{x}} & 0 & 0 \\ 0 & \varepsilon_{\hat{y}\hat{y}} & 0 \\ 0 & 0 & \varepsilon_{\hat{z}\hat{z}} \end{bmatrix} = \begin{bmatrix} 6.03 & 0 & 0 \\ 0 & 6.01 & 0 \\ 0 & 0 & 5.03 \end{bmatrix}. \tag{8}$$

$$[\varepsilon_{\text{r,ABS300}}] = \begin{bmatrix} \varepsilon_{\hat{x}\hat{x}} & 0 & 0 \\ 0 & \varepsilon_{\hat{y}\hat{y}} & 0 \\ 0 & 0 & \varepsilon_{\hat{z}\hat{z}} \end{bmatrix} = \begin{bmatrix} 2.93 & 0 & 0 \\ 0 & 2.92 & 0 \\ 0 & 0 & 2.85 \end{bmatrix}. \tag{9}$$

In the following, the effectively uniaxial anisotropic material described by the permittivity tensor in equations (8) and (9) is considered to be the host material from which the lens is manufactured and are assumed to be frequency independent. The desired effective permittivity distribution $\varepsilon_{\text{r,lens}}(x)$ and $\varepsilon_{\text{r,ml}}(x)$ are realized using periodic dielectric structures a with spatially modulated volumetric infill. In this work, we utilize the superposition of face-centered symmetric spatial harmonics as introduced in [3] to engineer the periodic structure to exhibit the desired effective permittivity for the GRIN lens $\varepsilon_{\text{r}}(x)$. A detailed description of these lattices is provided in [4] and omitted here for brevity's sake. Unit cells, created with the

[2] Material datasheets available from Avient upon request.

spatial harmonic superposition method, with lattice constant a and different threshold values th are depicted in Figure 3b.

Effective dielectric properties of the unit cells as a function of their volumetric infill are extracted via Floquet port scattering simulations as presented in [5]. The effective permittivity tensor components in non-dispersive frequency regimes are presented as a function of volumetric infill in Figure 3c. The effective permittivity tensor components are computed up to the maximum threshold value $\tilde{th}_{\max} = 0.625$ for which the lattices are still connected. Although a lattice with such a threshold value is theoretically possible, it would be quite fragile. Therefore, a maximum threshold value of $th_{\max}$ is used, which provides effective permittivity ranges of $\varepsilon_{\hat{x}\hat{x}} = \varepsilon_{\hat{y}\hat{y}} \in [2.5\ 6]$ and $\varepsilon_{\hat{z}\hat{z}} \in [2.25\ 5]$. Similar analysis is carried for the unit cells composed of the ABS300 material where a possible permittivity range of $\varepsilon_{\hat{z}\hat{z}} \in [1.25\ 2.85]$ is extracted.

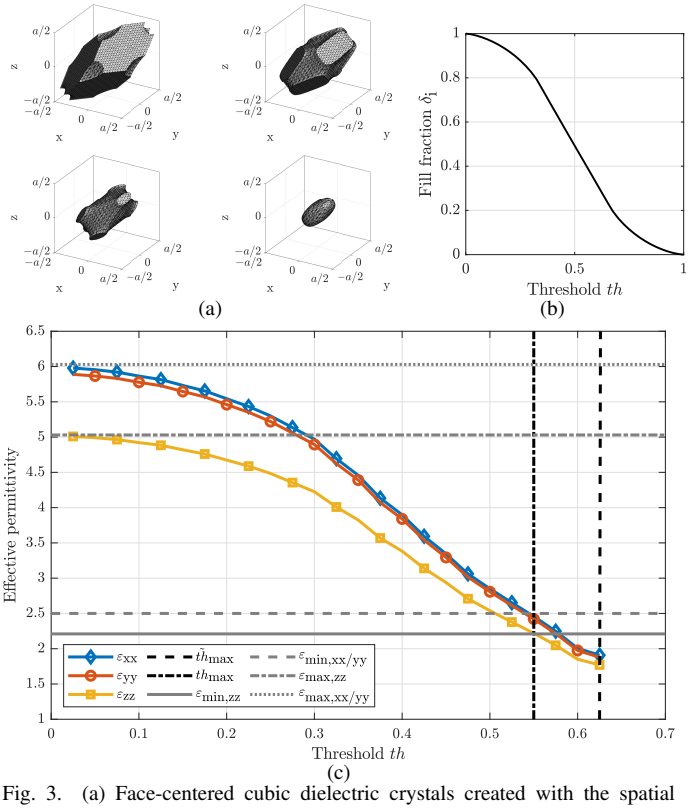

Fig. 3. (a) Face-centered cubic dielectric crystals created with the spatial harmonic superposition method for different thresholds (top-left) $th = 0.2$, (top-right) $th = 0.4$, (bottom-left) $th = 0.6$, and (bottom-right) $th = 0.8$ with the (b) relationship of the threshold and the unit cells volumetric infill ratio. (c) Effective permittivity tensor components of the FCC unit cells as a function of the threshold value with indication on the realizable values $\varepsilon_{\min}$ and $\varepsilon_{\max}$.

D. Final Lens Design

The lens design can now be finalized based on the extracted values of the minimum and maximum realizable permittivities above. This work considers a lens with a diameter $D = 45\text{mm}$ with an $F/D = 0.35$. Since the propagation through the lens is almost purely along the rotational axis of the lens, the effect of the dielectric anisotropy is neglected here, and the permittivities are considered to be isotropic with the respective values for $\varepsilon_{\hat{z}\hat{z}}$. Thus the minimum and maximum values for lens permittivities are $\varepsilon_{\text{r,max}} = 5$ and $\varepsilon_{\text{r,min}} = 2.25$. With this inputs to the design approach, the permittivity across the lens $\varepsilon_{\text{r}}(x)$, the permittivity in the matching layer $\varepsilon_{\text{r,ML}}(x)$ and the height of the matching layer $h_{\text{ML}}(x)$ are computed. The resulting values are depicted in Figure 4.

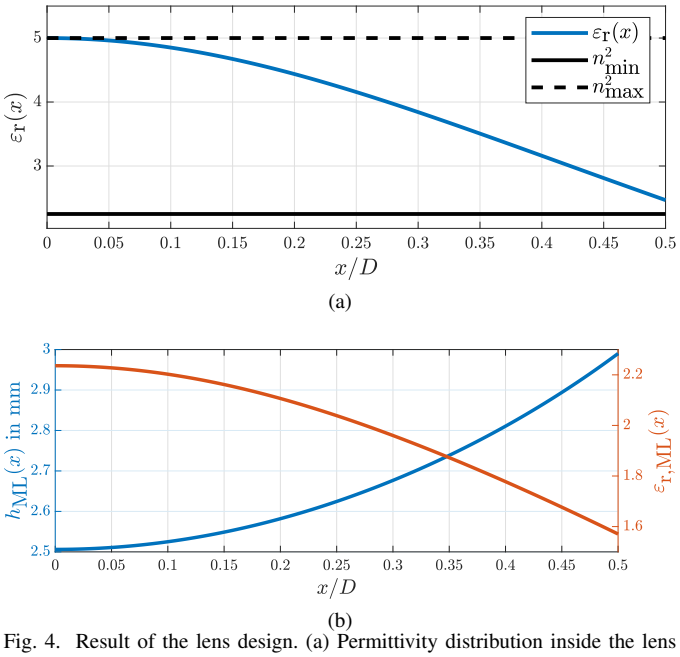

Fig. 4. Result of the lens design. (a) Permittivity distribution inside the lens core. (b) Permittivity distriubtion and height of the matching layer.

III. Manufacturing and Measurement

Manufacturing of the three prototypes is carried out on a core-XY 3D printer based on the E3D Toolchanger utilizing an E3D Hemera direct drive extruder and the ABS650 material from Avient in a 1.75mm filament format. An extrusion width of 0.2mm, a layer height of 0.12mm, and a print speed of $15\text{mm}\,\text{s}^{-1}$ is chosen. During the print, the model is oriented such that the rotational axis of the lenses z, as depicted in Figure 1, corresponds to the layer stack direction $\hat{z}$ of the printer as depicted in Figure 2. The manufactured lens prototypes with and without the matching layer, as depicted in Figure 5a, are experimentally verified in a benchtop anechoic chamber setup using an open-ended WR42 waveguide as the source. Measurements are carried out in the frequency range of $17 - 23\text{GHz}$ and angles off broadside θ between 0 and $90°$. Measured realized gain values are depicted in Figure 6 at broadside as a function of frequency and for discrete frequencies 19 and 21 GHz as a function of θ. The results demonstrate the desired collimating effect with the lens, which increases the realized gain of $\approx$ 10dB compared to the standalone waveguide. The lens with the integrated matching layer further increases the realized gain of $\approx 1.5\text{dB}$.

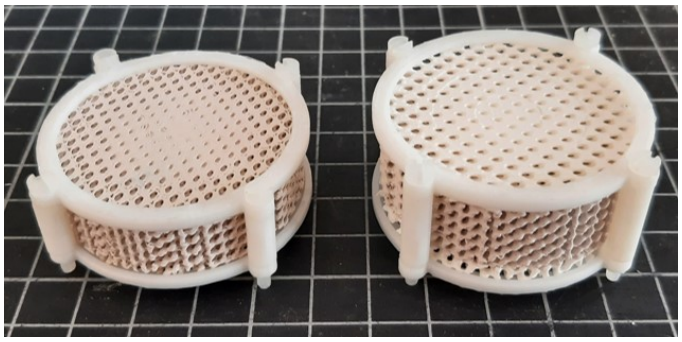

(a)

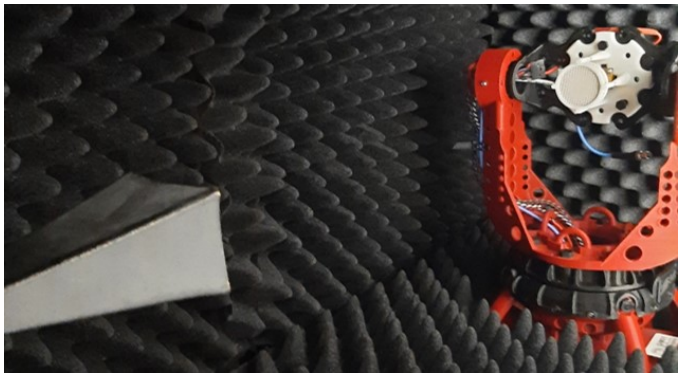

(b)

Fig. 5. (a) Manufactured lens prototypes with (right) and without (left) the matching layer inside holding structures for mounting in the measurement setup. (b) Lens mounted in the benchtop anechoic chamber for measurement.

IV. Conclusion

This work demonstrates the design, additive manufacturing, and experimental verification of a multi-material GRIN lens with an integrated matching layer operating at 20 GHz. To this end, we employ extrusion-based additive manufacturing to engineer a periodic dielectric structure with a spatially modulated volumetric infill for both the lens core and the matching layer. The lens design is carried out via an analytical evaluation of the optical path integral using the diameter and focal distance of the lens, as well as the maximum and minimum permittivities as inputs. The lens's permittivity range is extracted based on the selected print material and unit cell geometry. The effect of anisotropy in the print material is due to the layer-by-layer build approach, which was considered during the manufacturing but did not enter into the design of the lens. The manufactured prototypes are experimentally verified in a benchtop anechoic chamber using an open rectangular waveguide as the source. The experimental results demonstrate the desired collimation effect of the lens, and an increase in realized gain due to the integrated matching layer is confirmed.

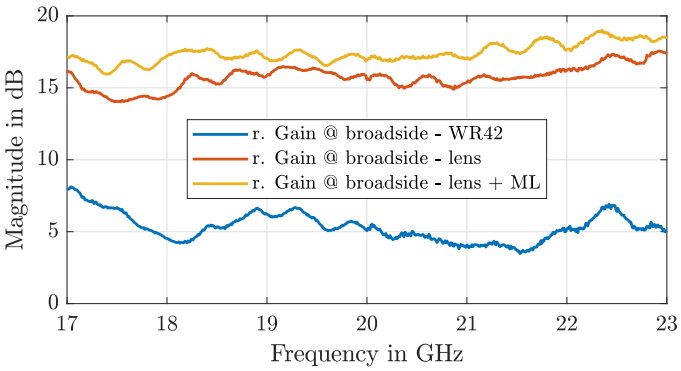

(a)

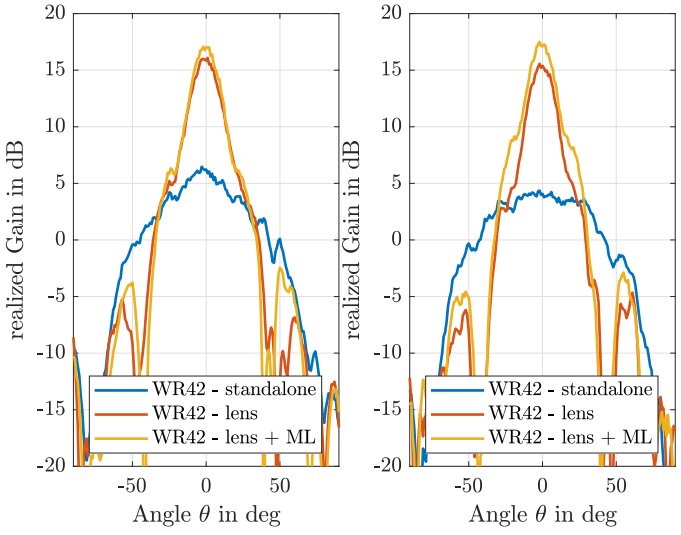

(b) (c)

Fig. 6. Comparison of measured realized gain values at (a) broadside as function of frequency and at (b) 19GHz and (c) 21GHz as function of angle θ off broadside.

References

[1] I. Munina, I. Grigoriev, G. O'donnell, and D. Trimble, "A Review of 3D Printed Gradient Refractive Index Lens Antennas," *IEEE Access*, vol. 11, pp. 8790–8809, 2023, ISSN: 2169-3536. DOI: 10.1109/ACCESS.2023.3239782 Accessed: Aug. 17, 2025. [Online]. Available: https://ieeexplore.ieee.org/document/10025721

[2] S. P. Hehenberger, S. Caizzone, and A. Yarovoy, "Modeling and measurement of dielectric anisotropy in materials manufactured via fused filament fabrication processes," *Materials Research Bulletin*, vol. 179, p. 112 938, Nov. 2024, ISSN: 0025-5408. DOI: 10.1016/j.materresbull.2024.112938 Accessed: Aug. 17, 2025. [Online]. Available: https://www.sciencedirect.com/science/article/pii/S0025540824002691

[3] R. C. Rumpf and J. Pazos, "Synthesis of spatially variant lattices," EN, *Optics Express*, vol. 20, no. 14, pp. 15 263–15 274, Jul. 2012, Publisher: Optica Publishing Group, ISSN: 1094-4087. DOI: 10.1364/OE.20.015263 Accessed: Aug. 17, 2025. [Online]. Available: https://opg.optica.org/oe/abstract.cfm?uri=oe-20-14-15263

[4] S. P. Hehenberger, A. P. T. Adithyababu, and S. Caizzone, "Effective Permittivity Measurement of 3D-Printed Dielectric Crystals," in *2022 16th European Conference on Antennas and Propagation (EuCAP)*, Mar. 2022, pp. 1–5. DOI: 10.23919/EuCAP53622.2022.9769370 Accessed: Aug. 17, 2025. [Online]. Available: https://ieeexplore.ieee.org/abstract/document/9769370

[5] S. P. Hehenberger, S. Caizzone, S. Thurner, and A. G. Yarovoy, "Broadband Effective Permittivity Simulation and Measurement Techniques for 3-D-Printed Dielectric Crystals," *IEEE Transactions on Microwave Theory and Techniques*, vol. 71, no. 10, pp. 4161–4172, Oct. 2023, ISSN: 1557-9670. DOI: 10.1109/TMTT.2023.3259479 Accessed: Aug. 17, 2025. [Online]. Available: https://ieeexplore.ieee.org/document/10089204